Synthesizing the Gulf Stream Thermal Structure from XBT Data*

MELINDA M. HALL

Physical Oceanography Department, Woods Hole Oceanographic Institution, Woods Hole, Massachusetts

(Manuscript received 30 April 1993, in final form 22 February 1994)

ABSTRACT

Thirty-six XBT temperature profiles have been used in a parametric model introduced by Hendry to model the Gulf Stream's thermal structure at 65°W between 200 and 1200 dbar, with an rms residual error of 0.56°C. Velocity has been computed geostrophically relative to 1200 dbar, and has been included in calculating potential vorticity analytically from the model. The resulting potential vorticity section for 65°W has been compared with the analogous result from Hendry's parametric model at 59°W, as well as observed potential vorticity sections from 68° to 55°W. There is a significant feature in the potential vorticity structure at 65°W not found at 59°W—namely, a relative minimum in potential vorticity along isopycnals, centered at the Gulf Stream's axis and 350 dbar. The modeled potential vorticity sections are consistent with the observations, including the downstream disappearance of this feature. The dynamical implications of these results are briefly discussed.

1. Introduction

Various authors (Hall and Bryden 1985; Hendry 1988; Hogg 1986, 1991) have used parameterizations of the Gulf Stream's (GS) thermocline temperature field, based on limited measurements, in order to correct current meter velocity and temperature time series to fixed standard depths. These parameterizations generally take advantage of the quasi-fixed or "canonical" nature of the field, at least for a given downstream location: the primary mode of variability for the GS thermocline is a simple horizontal translation, rather than internal deformation (Manning and Watts 1989; Halkin and Rossby 1985; Rossby 1987). Beyond their utility as correctional tools these parameterizations produce model GS thermoclines that can themselves be analyzed. Indeed, in his 1988 paper, Hendry suggests using them for regional intercomparisons of GS structure. The intent of this paper is to do precisely that using data collected in 1988.

During a hydrographic survey made as part of the Synoptic Ocean Prediction (SYNOP) Experiment (Hall and Fofonoff 1993), four XBT crossings of the GS were obtained between additional CTD and XBT sections at 68° and 55°W. Hall and Fofonoff (1993, hereafter HF93) have described in detail the observed GS structure from the CTD sections, but they did not discuss the XBT sections. Three of these, located from 67°–63°W, consisted entirely of T5 drops, which yield temperatures as deep as 1800 m; they were acquired within a time span of just over a day and crossed the "straight" portions of a trough/crest pair (Fig. 1a). This group of sections, comprising a total of 36 temperature profiles, has adequate vertical and cross-stream resolution to apply Hendry's model and obtain a smoothed GS thermocline, nominally at 65°W, for comparison with his 59°W section.

To make this comparison with Hendry's GS thermocline at 59°W, Hendry's (1988) method is applied to the set of XBT profiles centered around 65°W. In the next section, the model fit is derived in some detail, and the resulting analytical GS thermocline is compared with the XBT observations and with Hendry's 59°W section. In section 3, potential vorticity cross sections for this 65°W and Hendry's 59°W section are computed for intercomparison. In this paper, potential vorticity will be the dynamical quantity of particular interest, for it is what determines the current's inherent stability properties. Does the GS's canonical cross-stream structure change in potentially significant ways as we move downstream? The discussion places the results into a larger context by comparison with observations of GS potential vorticity at other locations along the stream as well. The final sections briefly summarize the conclusions of the overall study.

2. The model

A brief overview of Hendry's method, roughly following his notation, is as follows: First, each temperature profile was fit to a hyperbolic tangent function of pressure over a range of 200–1500 dbar,

$$T = A \tanh[B(C - p)] + D, \qquad (1)$$

* Woods Hole Oceanographic Institution Contribution Number 8394.

Corresponding author address: Dr. Melinda M. Hall, Woods Hole Oceanographic Institution, Woods Hole, MA 02543.

so that $A \tanh(BC) + D$ and $D - A$ bound the temperatures a given profile can represent (since $p > 0$ only); C is the "thermocline depth," where $\partial T/\partial p$ is a maximum; and B gives the scale depth of the thermocline. Next, parameters A, B, and D were fit to functions of C; namely,

$$A = \gamma e^{(-\delta C)} + \epsilon, \quad (2)$$

$$D = \alpha A + \beta, \quad (3)$$

$$B = a \operatorname{sech}[b(C - c)] + d, \quad (4)$$

and finally, with cross-stream distance y taken as the distance to the location of the 15°C isotherm at 200 m, parameter C was fit to

$$C(y) = -A_1 \tanh[B_1(C_1 - y)] + D_1, \quad (5)$$

where the subscript 1 is used to indicate that these are different from A, B, C, and D in (1). In (5), $A_1 + D_1$ and $D_1 - A_1$ give the maximum and minimum thermocline depths; B_1 is the scale width of the thermocline drop, that is, the current's deformation radius; and C_1 is an offset dependent on origin choice. Positive y values correspond to increasing distance onshore (northward) of the axis. Thus, x and u, the alongstream coordinate and velocity, are positive in the downstream direction, usually close to east; and y and v, the cross-stream coordinate and velocity, are positive in the "northward" direction, onshore. (In most of the literature on the Gulf Stream, the onshore side is shown to the left in figures of cross sections, so this convention is adopted for the figures in this paper.) The notation is admittedly confusing, but reference to Table 1 shows which of these parameters are constant rather than functions of y. Previous authors (e.g., Hogg 1986) have used the hyperbolic tangent $T(p)$ profile locally as a GS model; but the temperature range and scale depth of the GS thermocline change across the current, and this cross-stream structure must be included to obtain a realistic representation. (Clearly, it might be desirable to find a model depending on fewer than 13 parameters; however, the point of this paper is instead to provide another cross section to compare with Hendry's.)

Figures 1b,c show the collection of temperature profiles from the 36 XBT drops to be used in the model, and the temperature section versus alongtrack distance from southwest (right, 0 km) to northeast (left, 500 km). There are several temperature inversions associated with slope water intrusions on the cold "sides" as well as a deep, thickened 18°C Water layer. These features will contribute to the uncertainty in the final fits, but there is no good way to quantify their specific effect. Errors in fall rate for T5's are another source of uncertainty; because these errors have a greater relative effect deeper in the water column, where the net change of temperature is small across the GS at a given depth, the following fit includes values only between 200 and 1200 dbar, rather than 1500 dbar as Hendry used. Proceeding directly along Hendry's lines, each of the 36 temperature profiles was then fit to Eq. (1), yielding a collection of 36 values of A, B, C, and D corresponding to the 36 XBT profiles. (Meters and decibars are assumed interchangeable for the purposes of this note.) An initial fit of A to C was used to identify values lying more than 1.5 standard deviations from the fitted curve. This eliminated five points, and the remaining 31 stations were used to continue with the fits for $B(C)$ and $D(A)$; these fits had no outliers beyond two standard deviations (2.1 for D). Figures 2a,b,d show the fitted curves $A(C)$, $B(C)$, and $D(A)$; the 31 points to which the curves were fit; and the 5 outlier stations, plotted as open circles.

TABLE 1. Values of the 13 parameters in (2)–(5). The column labeled 65°W is for the XBT data discussed in this note; 59°W refers to Hendry's (1988) parameters.

	65°W	59°W
γ	10.84°C	8.92°C
δ	0.00958 dbar^{-1}	0.00912 dbar^{-1}
ϵ	7.326°C	7.230°C
α	0.938	0.942
β	4.829°C	4.830°C
a	0.00170 dbar^{-1}	0.00265 dbar^{-1}
b	0.00515 dbar^{-1}	0.00251 dbar^{-1}
c	658 dbar	557 dbar
d	0.00216 dbar^{-1}	0.00098 dbar^{-1}
A_1	326 dbars	322 dbar
B_1	−0.0260 km^{-1}	−0.0248 km^{-1}
C_1	−9.74 km	−10.60
D_1	437.4 dbar	445 dbar

To calculate cross-stream position y as the distance to 15°C at 200 m, one must define y for stations lying between two adjacent stream crossings—though C is fixed for such stations, the choice for y is clearly ambiguous. [Note that using a different definition, such as 12°C at 500 m as an origin, simply shifts the y coordinate uniformly by about 17 km, and does not remove the ambiguities noted above.] Between the first two sections, there was an overlap of two XBT drops; both of these yield similar (C, y) pairs, and both were included in the fit. However, between the second and third sections, we concluded on the basis of satellite IR data that we had not fully crossed the GS into the warm side before the isotherms rose again for the third section. There are four stations lying in the overlap region that might be used to define (C, y) pairs for the fit; two of these were included as "belonging to" the second section, and two to the third. These choices yield a group of 33 (C, y) values for the fit given by (5), and again this fit was good to within two standard deviations. Figure 2c shows the fit $C(y)$, the 33 points used for the fit, and the 5 points omitted from all the fits.

The rms error of the final $T(p, y)$ fit to the data for all 36 stations, between 200 and 1200 dbar, is 0.56°C, and for the 31 stations used in the fits, it is 0.50°C. The values of the 13 parameters are listed in Table 1,

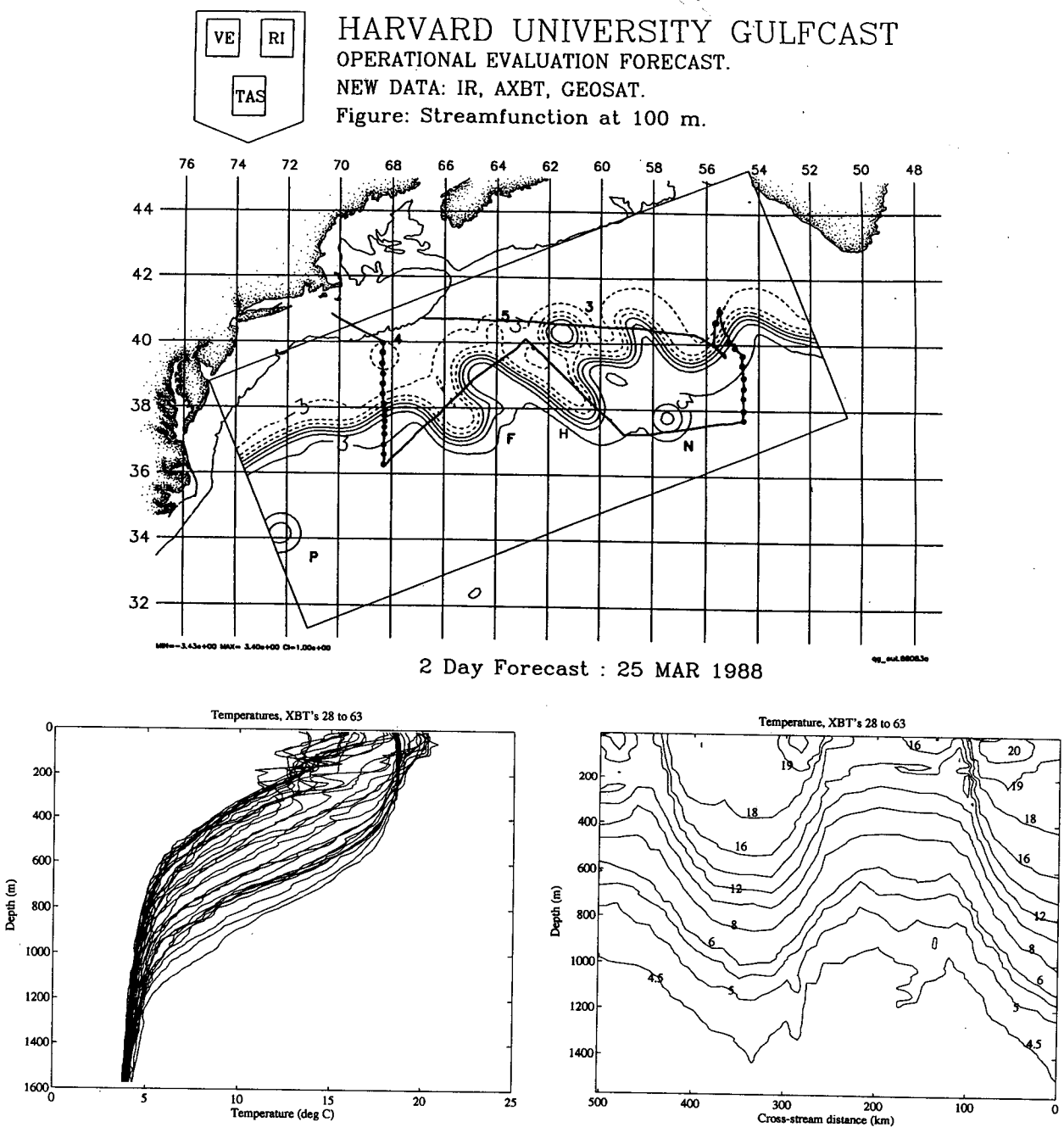

FIG. 1. (a) Harvard Gulfcast for 25 March 1988, with EN175 cruise track overlaid. (b) Temperature profiles for the 36 XBT drops used in the analysis. (c) Temperature contoured along the line of 36 XBT drops shown in panel b. Northeast is to the left, southwest to the right; cross-stream distance is equal to distance along the ship's track, which was virtually straight.

along with Hendry's (1988) values, and Fig. 3 compares the synthesized temperature field with the first XBT temperature section over a similar range of y. Except for north of the axis ($y > 0$), where the frontal aspect at temperatures $T \geqslant 14°C$ is smoothed by the model, it reproduces the temperature structure well: the synthetic field has a thermocline depth ranging from 112 to 763 dbar and reproduces temperatures ranging from 4.27° to 18.98°C between 0 and 1200 dbar. For comparison, Hendry's model thermocline varies from 123 to 767 dbar and has temperatures ranging from 4.32 to 18.79°C for 0–1200 dbar. The similarity is hardly surprising: Recall that A and D define the net temperature range of the current, whereas constants A_1 and D_1 in the fit for C give the net thermocline drop across the current, and B_1^{-1} is the deformation radius for the

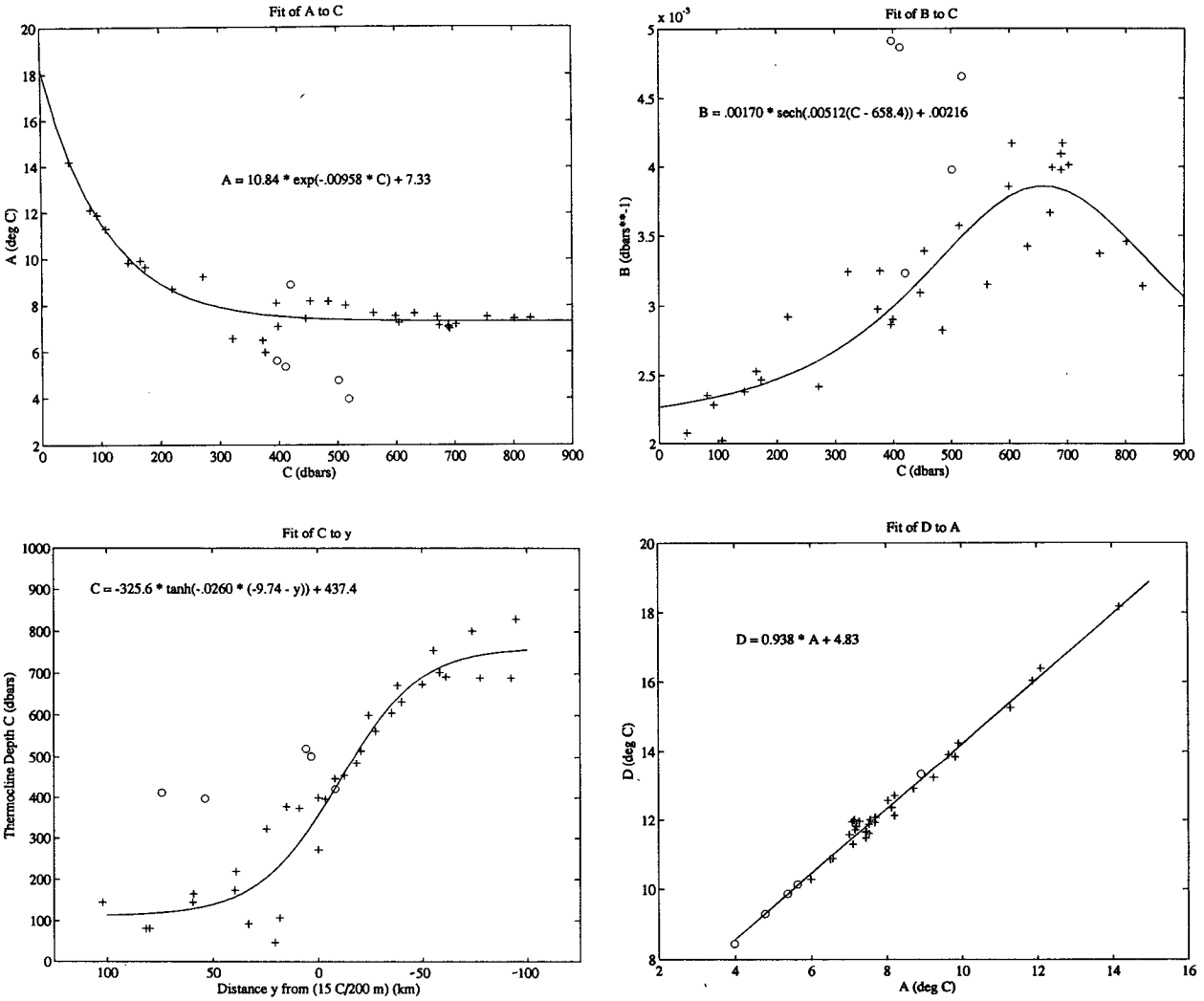

FIG. 2. (a) Fit of parameter A [Eq. (1)] to C, as given by Eq. (2). Pluses mark the values individually derived for each of the 31 stations used in the fit. Open circles are the values derived for the 5 stations omitted in the fit. (b) As in panel a but a fit of parameter B to C, as given by Eq. (4). (c) Fit of parameter C to y in Eq. (5). (d) As in panel a but a fit of parameter D to A, as in Eq. (3).

thermocline, approximately 38–40 km according to the values in Table 1. The constant parameter values in these three fits (Table 1) are only moderately different for the two sections, as one might expect, since such integral properties of the current are relatively constant going downstream.

In contrast, the local inverse scale depth for temperature is modeled by fit (4) for B, which is very different for the two sections; because C is a function of y, horizontal scales of variability are implicit in $B(C)$ as well, even though $C(y)$ is similar for the two sections. Figure 4 shows $[B(C(y))]^{-1}$ explicitly as a function of y across the current for 65° and 59°W: not only are the extrema [given by d, $a + d$ in (4)] farther apart at 65° than at 59°W, but the cross-stream distance over which most of the change occurs is slightly less at the former as well, leading to a steeper profile for B^{-1} overall. As will be seen in section 3, the stronger character of the increase of B (decrease of B^{-1}) at 65°W leads to a significant PV feature that is absent at 59°W; and we will see that the feature is robust to errors in the fit.

Geostrophic velocities may be calculated using

$$\frac{\partial u}{\partial z} = \frac{-g\alpha_0}{\rho_0 f}\frac{\partial T}{\partial y} \qquad (6)$$

$$\alpha_0 = 10^{-1}\ \text{kg m}^{-3}\ ^\circ\text{C}^{-1},$$

where T is used as a proxy for σ_θ and α_0 is the proportionality constant. Keeping in mind the resolution of the front, and that T is not a particularly good proxy for density when $T \geq 12$°C (especially on the cold side), the resulting velocity field nevertheless reproduces features typical of GS velocity sections, such as exhibiting a southward shift with depth of the velocity

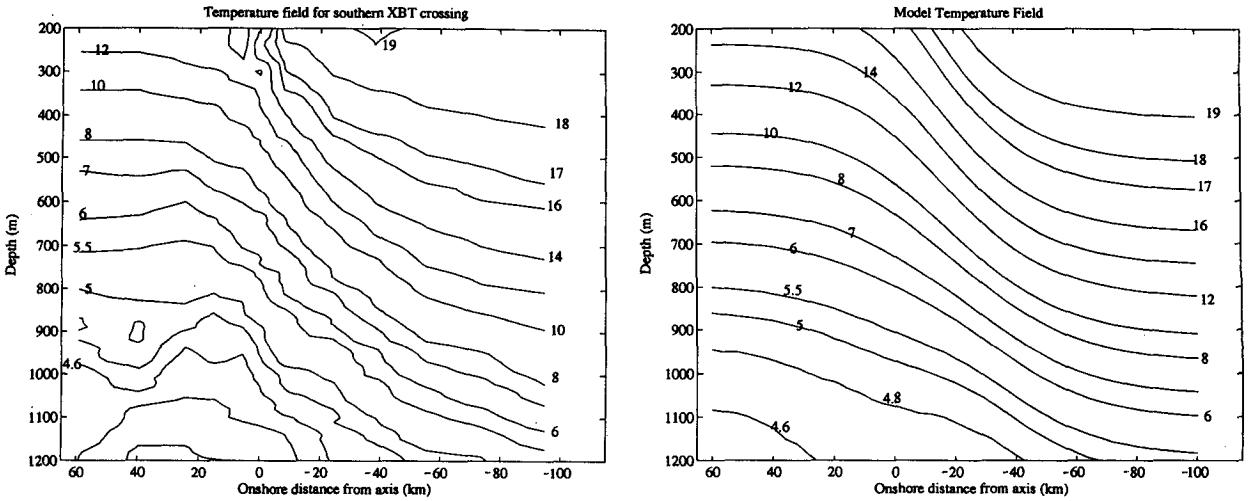

FIG. 3. (a) Temperature contoured for the southernmost XBT section in Fig. 1a, where $y = 0$ is the station location where $T \approx 15°C$ at 200 dbars. (Positive y values are onshore and are shown to the left.) (b) The model temperature contours over a similar range of y.

maximum. Table 2 makes a quantitative comparison of maximum velocities u_{max}, and transports in depth ranges, for the model and the observations: model values for transport are intermediate among the observations, while u_{max} is on the low side, probably because it occurs within the front. Transports for Hendry's model at 59°W are again similar to results at 65°W, because these depend on the net drop of isotherms across the current rather than local variability.

We now turn to the PV structure of the current, which is of greater dynamical interest.

3. Potential vorticity

An analytic model is useful for examining a highly derived quantity such as the potential vorticity (PV)

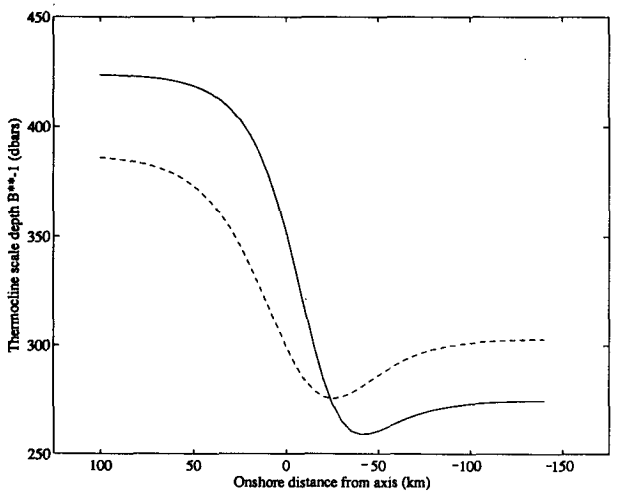

FIG. 4. Comparison of the fits at 65° (solid) and 59°W (dashed) for B, shown explicitly as a function of the cross-stream position y. The inverse of B, which is the local scale depth for temperature, is plotted.

structure associated with the temperature field, since the calculation can be done analytically for the most part. As noted above, temperature has been used as a proxy for density σ_θ using a fixed value α_0 of the proportionality constant; thus, potential vorticity Π can be calculated using σ_θ as the conservative tracer in the expression for Π, for comparison with HF93. To review, the full PV Π of a water parcel is then given as

$$\Pi = \frac{-1}{\rho_0}(2\Omega + \omega_{rel}) \cdot \nabla\sigma_\theta \qquad (7)$$

(e.g., Pedlosky 1979), where 2Ω is planetary vorticity and ω_{rel} is the (three-dimensional) relative vorticity of the flow. The minus sign ensures positive values of Π in the Northern Hemisphere for large-scale flow. In quasigeostrophic theory, (7) reduces to

$$\Pi = \frac{-1}{\rho_0}\left(f + \frac{\partial v}{\partial x} - \frac{\partial u}{\partial y}\right)\frac{\partial \sigma_\theta}{\partial z}, \qquad (8)$$

and in the eastward GS, $v_x \ll u_y$, so that term may be dropped. However, because isopycnals depart significantly from being horizontal, a nonquasigeostrophic term must also be retained from the dot product in (7); namely,

$$\frac{-1}{\rho_0}\frac{\partial u}{\partial z}\frac{\partial \sigma_\theta}{\partial y}$$

(scale analysis can be used to show that this term may be of the order of

$$\frac{-1}{\rho_0}\frac{\partial u}{\partial y}\frac{\partial \sigma_\theta}{\partial z},$$

see HF93). The expression for Π then becomes, as in HF93,

TABLE 2. Comparison of transports (10^6 m^3 s^{-1}) in depth ranges and maximum velocities for the three XBT crossings and for the model sections at 65° and 59°W.

Depth range (m)	Section 1 (XBT 28–41)	Section 2 (XBT 40–53)	Section 3 (XBT 50–63)	Model	
				65°W	59°W
200–400	14.8	10.6	10.0	14.2	14.0
400–600	10.6	6.8	6.5	8.6	8.6
600–800	6.0	3.2	3.1	3.8	4.1
800–1000	2.6	1.2	1.1	1.1	1.4
1000–1200	0.5	0.3	0.2	0.2	0.3
200–1200	34.5	22.0	20.9	27.9	28.4
u_{max} (cm s^{-1})	169	104	133	110	111

$$\Pi = \frac{-1}{\rho_0}\left(f - \frac{\partial u}{\partial y}\right)\frac{\partial \sigma_\theta}{\partial z} - \frac{1}{\rho_0}\frac{\partial u}{\partial z}\frac{\partial \sigma_\theta}{\partial y}$$

$$= \frac{-1}{\rho_0}\left(f - \frac{\partial u}{\partial y}\right)\frac{\partial \sigma_\theta}{\partial z} - \frac{g^2}{\rho_0^2 f}\left(\frac{\partial \sigma_\theta}{\partial y}\right)^2 \qquad (9a)$$

or, using (6) and writing (9a) in terms of temperature,

$$\Pi = \frac{\alpha_0}{\rho_0}\left(f - \frac{\partial u}{\partial y}\right)\frac{\partial T}{\partial z} + \frac{\alpha_0}{\rho_0}\frac{\partial u}{\partial z}\frac{\partial T}{\partial y}$$

$$= \frac{\alpha_0}{\rho_0}\left(f - \frac{\partial u}{\partial y}\right)\frac{\partial T}{\partial z} - \frac{g\alpha_0^2}{\rho_0^2 f}\left(\frac{\partial T}{\partial y}\right)^2. \qquad (9b)$$

One may add a barotropic velocity component at 1200 dbar if desired, but leaving it out in subsequent calculations does not affect the qualitative structure of the PV fields. Therefore, only baroclinic velocities relative to 1200 dbar are included in what follows. In the definition (9) of Π, the only term that is not easily calculable analytically is $\partial u/\partial y$, since obtaining the geostrophic velocity in the first place involves integration with depth; it is far simpler (and adequately accurate) to calculate this term by differencing.

The PV fields have been calculated for this section and for Hendry's, using the parameter values of Table 1 and Eqs. (6) and (9); they are shown in Figs. 5a and 6a. It is important to recognize that a density-conserving water parcel in the current locally feels the PV distribution along isopycnals. Therefore, several representative isotherms have been superposed on the PV in Figs. 5 and 6, to give the reader an idea of how the cross-stream PV structure, as viewed by water parcels, varies from one part of the thermocline to another. Several other comments are in order regarding the three different components contributing to Π in (9). First, note that f, u_y, and $\partial\sigma_\theta/\partial z$ all vary across the stream; changes in the product $f(\partial\sigma_\theta/\partial z)$ are dominated by changes in $\partial\sigma_\theta/\partial z$, and β is insignificant compared to the relative vorticity. Thus the term proportional to $f(\partial\sigma_\theta/\partial z)$ (or fT_z) is referred to as the stretching component since it mainly reflects compression and stretching of isopycnals (isotherms). In contrast, changes in $-u_y(\partial\sigma_\theta/\partial z)$ are dominated by the change in the relative vorticity $-u_y$ itself. This term is referred to as the relative vorticity component and it reinforces stretching north of the axis, the cyclonic side, but reduces it on the anticyclonic side where $-u_y$ is negative. The third term will be called the nonquasigeostrophic (non-QG) term and is everywhere negative. It is strongest just north of the velocity maximum, and like the velocity field, its maximum slopes southward with depth. The stretching component dominates PV structure at both sections, as demonstrated by comparison of Figures 5a and 6a (total PV) with 5b and 6b (stretching PV). The relative and non-QG contributions are of comparable magnitude to one another, as much as 25% as great as the stretching terms; because of their characteristic structures, they tend to cancel in the cyclonic portions of the current and reinforce one another on the anticyclonic side.

The GS has long been recognized, and modeled, as a strong PV front, separating less strongly stratified, low PV Sargasso Sea water from more stratified higher PV slope water. This structure is visible but not prominent in Figs. 5 and 6 because the strongest part of the front lies above 200 m, and is largely due to the transition to slope water T/S characteristics, not accounted for by the model. A more complex structure is striking at 65°W (Fig. 5), namely, a pronounced minimum along isotherms located near the axis at a depth of about 350 m. Notice that this minimum is inherent in the vertical density structure alone (Fig. 5b), for its appearance does not depend on the inclusion of the relative and nonquasigeostrophic terms of Π, although the latter tends to enhance it. Figure 5c shows total PV values along the 12.9°C isotherm (the 200 dbar temperature at $y = 60$ km), which passes through the minimum. At 59°W, this 350-m axis minimum is absent in the total PV, though in fact the sum of the stretching and non-QG terms alone displays it; but there is a deeper minimum centered at 700 m about 50 km south of the axis, a feature hinted at in Fig. 5a for 65°W by the slight pinching of PV contours at that same depth, again 50 km offshore of the axis. Below temperatures

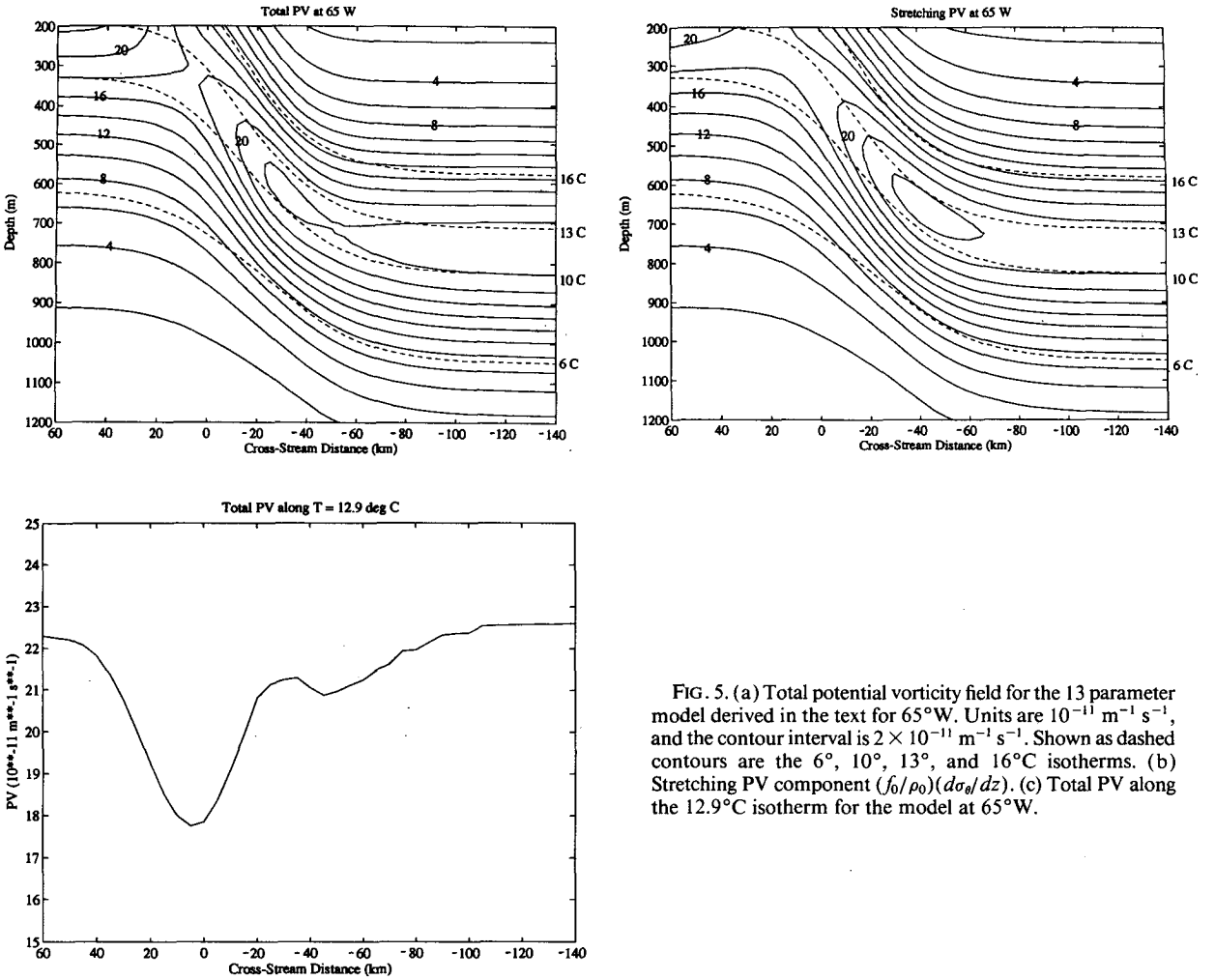

FIG. 5. (a) Total potential vorticity field for the 13 parameter model derived in the text for 65°W. Units are 10^{-11} m^{-1} s^{-1}, and the contour interval is 2×10^{-11} m^{-1} s^{-1}. Shown as dashed contours are the 6°, 10°, 13°, and 16°C isotherms. (b) Stretching PV component $(f_0/\rho_0)(d\sigma_\theta/dz)$. (c) Total PV along the 12.9°C isotherm for the model at 65°W.

of 7°–8°C at both sections, PV remains approximately uniform along isotherms.

First consider how well the model reproduces observed PV in the GS. In Fig. 7, the PV section of HF93 at 68°W has been replotted and smoothed using three contours [10, 20, and 25 ($\times 10^{-11}$ m^{-1} s^{-1})] to highlight its key features; it is shown over a y, z range comparable to that in Figs. 5 and 6. (The current axis $y = 0$ corresponds to the location of station 7 in HF93's figures.) Although the plot is noisy, there is a clear break in strong values near the axis, though it is some 100 m deeper than the corresponding minimum in the synthesized section at 65°W. HF93 identified this single minimum, and associated it with densities of $\sigma_\theta = 26.4$–27.1 kg m^{-3} ($\theta = 11°$–18°C). Figure 7 of this paper, rather less cluttered than Fig. 9a of HF93, suggests that the minimum occurs in a deeper range of σ_θ (perhaps 26.9–27.4 kg m^{-3}, $\theta = 8°$–13.5°C); moreover, at 40–50 km offshore of the axis between 600 and 700 m, there indeed appears to be another relative minimum like the one seen in the model PV at 59°W.

Relative to the density range and current axis, the location of the shallower minimum also agrees closely with that pictured in Bower et al. (1985). Their PV section at 68°W (their Fig. 1d), calculated only from density data, shows the axis minimum and offshore relative maximum at densities $\sigma_\theta = 27.0$–27.5 kg m^{-3}. They do not find the weaker and deeper secondary minimum, but this is not surprising, as this feature depends on the inclusion of terms other than the stretching (cf. Figs. 6a and 6b). For the model at 65°W, the PV contrast between the minimum and the higher values to north and south (along an isotherm) is approximately equal, about 4–5 ($\times 10^{-11}$ m^{-1} s^{-1}) (Fig. 5c). The observations at 68°W show the contrast going onshore (northward) to be much greater than that going offshore, about 25×10^{-11} m^{-1} s^{-1} compared to 5–10 ($\times 10^{-11}$ m^{-1} s^{-1}) (HF93). The discrepancy of course is due to the fact that the model does not reach the high values of PV northward of the axis, as noted above. It is further interesting that according to observations the shallow minimum does not seem to persist

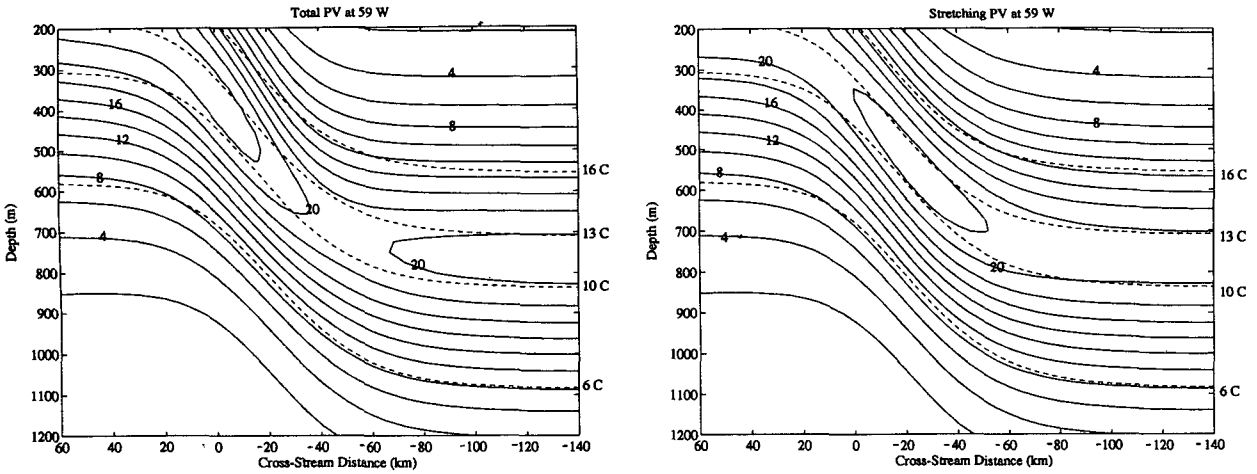

FIG. 6. Same as in Fig. 5 but for Hendry's parametric model at 59°W.

downstream: it is barely evident in the Bower et al. 64°W section and is absent entirely in their sections farther downstream; nor was it found in the 55°W CTD section (see HF93). This is consistent with its absence in Hendry's model PV structure for 59°W (Fig. 6a), though the weaker offshore minimum at $y \approx 50$–60 km persists. As noted above, the latter is due to the combined effect of the last two terms on the right-hand side of (7), both of which are due to the flow and are negative south of the axis.

We return to the dynamical importance of this specific PV structure momentarily, but consider first how errors in the fits could modify the results. The similarity of the parameters in the fits for A, D, and C at the two locations reflect the persistent downstream coherence of the GS's thermocline structure. Indeed, one could do a reasonable job of selecting these fits simply by careful examination by eye of the observed temperature structure. Quantitatively, as well, the model is insensitive to changes in these fits: substituting the 59°W fits for A, D, C at 65°W, the rms error over the 36 stations, between 200 and 1200 dbar, increases only to 0.59°C (from 0.56°C). Qualitatively, a substitution for A and D, or for C, alone does not affect the PV structure substantially.

By contrast, changes to the fit for the local inverse scale depth B more strongly affect the model. Quantitatively, holding the fits for A, D, C but substituting 59°W parameters for B increases the rms error in temperature to 0.62°C. More significantly, this substitution completely eliminates the relative minimum at 350 m seen in the model PV. To examine this point further, the constant parameters in the fit for B were varied smoothly so that the steeper 65°W curve in Fig. 4 gradually approached the shape at 59°W, while holding the fits for A, D, and C at their 65°W values. The relative minimum in PV persists, retreating upward and northward as the 59°W curve for B is approached. However, the values of a, b, c, and d in (4) must be changed over 90% of the way from the 65°W to the 59°W values before the minimum disappears altogether. Indeed, the fitted curve for B as given by the parameter values in Table 1 is significantly better than a fit using altered values: when altered values (90% of the way toward the 59°W values) are used, the standard deviation of the difference between predicted and fitted values of $B(C)$ over 31 points is 50% greater than when the values in Table 1 are used. Furthermore, over most of the range of C, the two curves differ by an amount greater than the standard deviation of the original fit.

We now return to the dynamical significance of features in the PV field. It was noted that the current's stability properties depend on its PV structure. In particular, away from the influence of top and bottom boundaries, the PV gradient $\partial \Pi / \partial y$ must change sign somewhere within the current for instabilities to be possible. Now in a flow where density is conserved following fluid parcels, the appropriate gradient Π_y to consider is that calculated along isopycnals (in quasi-geostrophic theory this is the same to lowest order as Π_y along constant z, but in the GS isopycnals depart from horizontal). Following the PV structure along the isotherms superposed in Fig. 5a, we see that at temperatures below about 9°C and above 14°C Π is nearly uniform along isotherms. However, midthermocline isotherms, such as that shown in Fig. 5c, pass through some part of the minimum, and hence along these, the gradient of Π does change sign.

Theoretical work by Pratt et al. has investigated the dynamics of a current with such a PV structure, modeling the flow as a midlatitude jet with piecewise uniform PV. [Note that because the axis minimum is present in the stretching component alone, it is a fundamental feature of the GS and it is thus appropriately

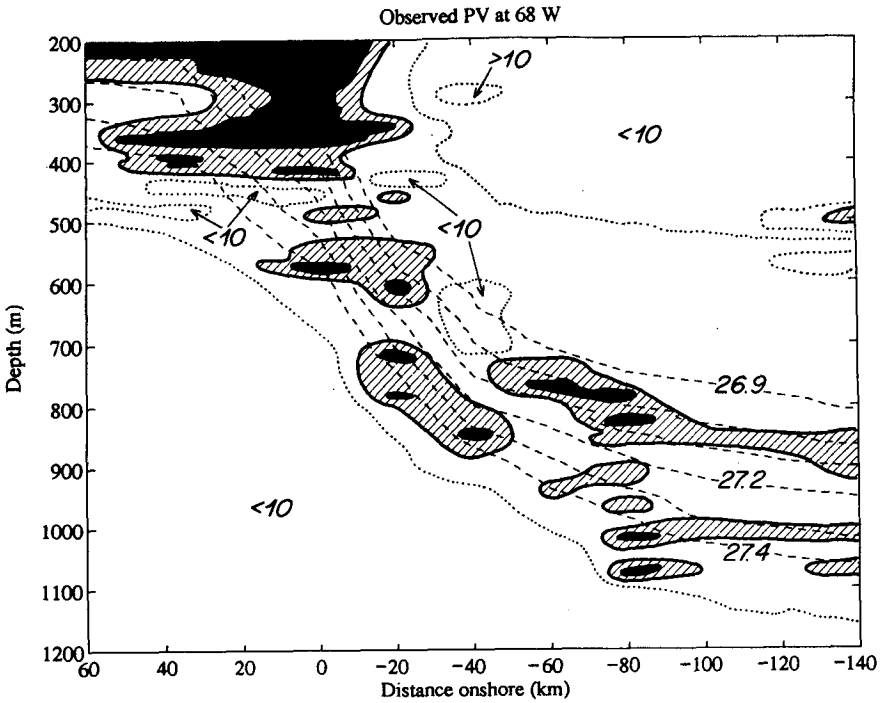

FIG. 7. Observed PV at 68°W, adapted from Hall and Fofonoff (1993) and displaying only the 10, 20, and 25 × 10^{-11} m^{-1} s^{-1} contours. Solid areas are greater than 25 × 10^{-11} m^{-1} s^{-1}; hashed areas are 20–25 × 10^{-11} m^{-1} s^{-1}; dotted contour is the 10 × 10^{-11} m^{-1} s^{-1} contour. Dashed contours are isopycnals from σ_θ = 26.9 kg m^{-3} to σ_θ = 27.4 kg m^{-3} with a contour interval of 0.1 kg m^{-3}.

included at lowest order in such a model.] They found that when the PV contrast at the southern edge of the minimum is O(20%–50%) the magnitude of the contrast north of the minimum, instabilities develop on the southern side of the current, which resemble the "warm outbreaks" described by Cornillon et al. (1986), in which warm, shallow Gulf Stream water (as opposed to slope water) is ejected into the Sargasso Sea. These outbreaks are observed only south of the stream and occur only west of 65°W. At 68°W, the PV contrast falls within the range necessary for instability (HF93), though in the synthesized section at 65°W the northern contrast is underestimated for reasons cited above. At 59°W, the shallow minimum is absent, and indeed warm outbreaks do not seem to occur this far east. Indeed, the Pratt et al. (1991) model is inappropriate for investigating the dynamics of the deeper minimum found in the synthesized PV at 59°W because that minimum arises from terms not accounted for in the model.

4. Conclusions and implications

Following a method introduced by Hendry (1988), 36 XBT temperature profiles near 65°W have been used to model the GS thermocline there between 200 and 1200 dbar. The model allows the temperature range and scale depth of the thermocline to vary as a function of thermocline depth, which in turn is a function of cross-stream position in the current. This 65°W model section has been compared with Hendry's analogous result at 59°W: the quantitative similarity of most of the constant parameters in the fits for the two models reflects the downstream persistence of the GS bulk canonical structure, including minimum and maximum temperatures, minimum and maximum thermocline depths, predicted baroclinic transport relative to 1200 dbar, and the current's deformation radius. There is a marked difference, however, in the cross-stream variation of the scale depth for temperature at the two sections, which leads to a significant difference in the potential vorticity structure computed from the model at the two locations. In particular, at 65°W there is a relative minimum along midthermocline isopycnals near the GS axis at 350 dbar that does not appear in the downstream section. This minimum is evidently a robust feature of the GS's PV near 68°W, inherent in the density structure of the current, and enhanced by the inclusion of a nonquasigeostrophic term in the expression for PV. Overall, the modeled PV structure for the GS at 65° and 59°W and the downstream modification they imply is consistent with observed PV sections between 68° and 55°W. At 59°W there is a deeper relative minimum 50 km south of the

axis, not seen in the observations of Bower et al. (based on density alone), because it derives from the relative vorticity and nonquasigeostrophic contributions to the PV.

The difference in the types and locations of relative minima and maxima at 65° and 59°W suggests that the nature of instabilities arising in the GS can vary as a function of longitude. One example is the warm outbreaks (Cornillon et al. 1986) observed primarily west of 65°W, which according to theoretical work by Pratt et al. (1991) could arise in a jet with the PV structure observed at 68° and 65°W. Alternatively, the cross-stream variation of the temperature scale depth may change in time as a result of meanders or ring interactions distorting the thermocline, that is, steepening it or spreading it out. Manning and Watts (1989) have identified two important modes of thermocline variability other than translation, that could have such an effect. Their so-called transport mode is associated with a net increase in the drop of the thermocline across the current, and their "vorticity mode" with a change in horizontal shear. The first would certainly change the fit for $C(y)$, and the second might affect any of the fits. Such changes are likely to affect the axis minimum in PV, suggesting that temporal variability in the current's stability properties could result as well.

Acknowledgments. My involvement in the SYNOP program has been greatly enriched by continuing interactions with the many individuals who have contributed to this group effort. I also thank anonymous reviewers whose comments vastly improved the final version of this work. This work was supported by ONR Contract N00014-87-K-0001, NR 083-004, and ONR Grants N00014-88-K-0612 and N00014-89-J-1056.

REFERENCES

Cornillon, P. D., D. Evans, and W. Large, 1986: Warm outbreaks of the Gulf Stream into the Sargasso Sea. *J. Geophys. Res.*, **91,** 6583–6596.

Halkin, D., and T. Rossby, 1985: The structure and transport of the Gulf Stream at 73°W. *J. Phys. Oceanogr.*, **15,** 1439–1452.

Hall, M. M., and H. L. Bryden, 1985: Profiling the Gulf Stream with a current meter mooring. *Geophys. Res. Lett.*, **12,** 203–206.

——, and N. P. Fofonoff, 1993: Downstream development of the Gulf Stream from 68° to 55°W. *J. Phys. Oceanogr.*, **23,** 225–249.

Hendry, R. M., 1988: A simple model of the Gulf Stream thermal structure with application to analysis of moored measurements in the presence of mooring motion. *J. Atmos. Oceanic Technol.*, **5,** 328–339.

Hogg, N. G., 1986: On the correction of temperature and velocity time series for mooring motion. *J. Atmos. Oceanic Technol.*, **3,** 204–214.

——, 1991: Mooring motion corrections revisited. *J. Atmos. Oceanic Technol.*, **8,** 289–295.

Manning, J. P., and D. R. Watts, 1989: Temperature and velocity structure of the Gulf Stream northeast of Cape Hatteras: Modes of variability. *J. Geophys. Res.*, **94**(C4), 4879–4890.

Pedlosky, J., 1979: *Geophysical Fluid Dynamics.* Springer-Verlag, 624 pp.

Pratt, L. J., J. Earles, P. Cornillon, and J.-F. Cayula, 1991: The nonlinear behavior of varicose disturbances in a simple model of the Gulf Stream. *Deep-Sea Res.*, **38**(Suppl. 1A), S591–S622.

Rossby, T., 1987: On the energetics of the Gulf Stream at 73°W. *J. Mar. Res.*, **45**(1), 59–82.